



Cite this: *Biomater. Sci.*, 2022, **10**, 6707

Development of a hydrocolloid bio-ink for 3D bioprinting

Özüm Yildirim  and Ahu Arslan-Yildiz *

A new generation of bio-inks that are soft, viscous enough, stable in cell culture, and printable at low printing pressures is required in the current state of 3D bioprinting technology. Hydrogels can meet these features and can mimic the microenvironment of soft tissues easily. Hydrocolloids are a group of hydrogels which have a suitable gelling capacity and rheological properties. According to the literature, polysaccharide-based hydrocolloids are used in the food industry, wound healing technologies, and tissue engineering. Quince seed hydrocolloids (QSHs), which consist of mostly glucuronoxylan, can easily be obtained from quince seeds by water extraction. In this study, the use of a QSH as a bio-ink was investigated. The suitability of QSH for the printing process was assessed by rheological, uniformity and pore factor analyses. Appropriate printing parameters were determined and the characterization of the bioprinted QSHs was performed by SEM analysis, water uptake capacity measurement, and protein adsorption assay. The bioprinted QSHs had excellent water uptake capacity and showed suitable protein adsorption behaviour. Analyses of the biocompatibility and cellular viability of bioprinted QSHs were conducted using NIH-3T3 fibroblast cells and the results were found to be high during short and long-term cell culture periods. It was proved that QSH is a highly promising bio-ink for 3D bioprinting and further tissue engineering applications.

Received 27th July 2022,
Accepted 6th October 2022

DOI: 10.1039/d2bm01184k

rsc.li/biomaterials-science

Introduction

Bioprinting is an emerging methodology for the fabrication of three dimensional (3D) tissue models in an automated way with a desired shape, dimension, controllable pore size and distribution.^{1–4} With these advantages, bioprinting overcomes the limitations of biofabrication and allows the production of 3D tissue-like constructs with pre-programmed configurations, biomaterials and/or cells.^{2,5–7} Bio-ink is one of the most important components of the bioprinting process and has the utmost importance in the success of bioprinting. However, obtaining a high-performance bio-ink is still a challenging endeavor for the research community. Bio-inks should be soft, fluid, viscous enough to be easily printed during the printing process, tough enough to maintain the printed pattern after the printing process,^{8,9} and stable in cell culture media during the culturing process.⁵ In addition, bio-ink materials should be biocompatible and non-toxic since cells will be encapsulated in them,¹⁰ where bio-inks should promote cell adhesion and proliferation. Bio-inks are also supposed to be easily processed, cost-effective, and commercially available.¹¹ However,

it is observed that the materials used in bioprinting applications cannot provide all these features together.⁸

The development of new-generation bio-inks is an important challenge that needs to be addressed in the field of tissue engineering and 3D bioprinting. New-generation bio-inks are required, which have the required viscosity features, physicochemical and mechanical properties, high biocompatibility, easy and non-toxic cross-linking, low cost, and high availability.^{12,13}

Hydrogels mostly have these features as well as the ability to mimic the microenvironment of soft tissues; therefore, they are widely used as bio-ink materials in bioprinting applications.^{11,14,15} Hydrocolloids are a group of hydrogels, which have significant rheological and viscosity properties.^{16,17} Polysaccharide-based hydrocolloids are one of the biggest classes of natural hydrocolloids that have biocompatibility, biodegradability, and gelling features. With these advantages, they are generally used in drug release,^{18–20} wound healing^{21,22} and tissue engineering applications as a scaffold material.²³ Hydrocolloids are among the promising natural materials for tissue engineering applications and the development of new-generation bio-inks, with their water solubility, biocompatibility, high water retention capacity,²⁴ biodegradability, anti-inflammatory and antioxidant properties.^{25,26}

Here, a polysaccharide-based hydrocolloid was obtained from quince seeds and has been used as a new-generation bio-ink in 3D bioprinting. The quince-seed hydrocolloid (QSH) has

Department of Bioengineering, Izmir Institute of Technology (IZTECH), 35430 Izmir, Turkey. E-mail: ahuarslan@iyte.edu.tr

good gelling capability based on its high polysaccharide content, which is mostly glucuronoxylan.^{27–29} The quince-seed hydrocolloid, obtained by gelling the quince seed with water, is a promising tissue scaffold material in terms of its mechanical and physicochemical properties, as well as biocompatibility. According to the literature, there are a number of studies that examine the mechanical and rheological properties of quince seed hydrocolloids.^{30,31} Recently we have demonstrated the capability of quince seed hydrocolloids as a tissue engineering scaffold, which shows high biocompatibility and favors 3D tissue model formation.²⁶ In this study, a new polysaccharide-based hydrocolloid bio-ink from quince seed was used in 3D bioprinting and cell-laden formation. For this purpose, the printability parameters of the water extracted QSH were analyzed to investigate the performance of the bio-ink. Characterization and shape-fidelity analysis of the bioprinted QSH construct were performed through analysis of linear and pore regularity and SEM analysis. Besides, the bioprinted hydrocolloid construct was investigated in terms of water uptake and protein adsorption capacity. The use of QSH as a bio-ink was evaluated using MDA-MB-231 GFP and NIH-3T3 fibroblast cell-printed constructs. Furthermore, the cell viability and proliferation profiles of NIH-3T3 fibroblast cells were investigated. Here, for the first time it is demonstrated that the QSH has great potential as a bio-ink that is capable of providing a suitable microenvironment for 3D cell culture formation and can be used for further bioprinting applications.

Experimental

Materials

An Axodual 3D-Bioprinter (AxolotlBio Systems) was used for printing cell-laden constructs. Quince seeds were extracted from quince fruits collected in the western side of Turkey. 1-Ethyl-3-(3-dimethylaminopropyl) carbodiimide (EDC) and *N*-hydroxysuccinimide (NHS) were purchased from Sigma Aldrich. Rhodamine B from Merck and fluorescein from Fluka Analytical were used for the visualization of bioprinted constructs by fluorescence microscopy. For protein adsorption assay, lyophilized powder bovine serum albumin (BSA) from Sigma Aldrich and sodium dodecyl sulfate (SDS) from Bioshop were purchased. Cell culture experiments were performed using trypsin-EDTA (sterile-filtered, 0.25%, BioReagent), penicillin-streptomycin (P/S), high glucose Dulbecco's modified Eagle's medium (DMEM), phosphate buffered saline (PBS, pH 7.4 10 \times), fetal bovine serum (FBS) from Gibco and dimethyl sulphoxide (DMSO) from Carlo Erba. MDA-MB-231 GFP cells³² and the NIH-3T3 mouse fibroblast cell line (ATCC® CRL-1658™) were used for bioprinting studies. CytoCalcein AM and Propidium Iodide dye (AAT Bioquest) were used for cell viability and live/dead assays.

Bio-ink preparation

The quince seed hydrocolloid (QSH) was prepared as described elsewhere.²⁶ Briefly, to prepare 40 mg mL⁻¹ QSH, 200 mg of

the outer shell of quince seeds was weighed and mixed with 5 mL of ultra-pure water including 100 μ L of either fluorescein or rhodamine B fluorescence dye, and gelation was completed after 24-hour incubation at room temperature. 50, 60 and 100 mg mL⁻¹ QSH were also prepared with 250, 300 and 500 mg quince seed shells, respectively. After the filtration step to remove the remaining seed particles, hydrocolloids were collected and stored at +4 °C until further use. Either rhodamine B or the fluorescein dye was used to facilitate the easy visualization of the bioprinted constructs.

EDC and NHS coupling methodology was applied for cross-linking QSHs during bioprinting. This crosslinking methodology provided amide bond formation between the carboxylic acid (-COOH) and amide (-CONH₂) groups that are found in the QSH structure.³³ In order to achieve EDC-NHS coupling, 200 μ L of EDC (0.4 M) and NHS (0.1 M) were added and homogenized in 1 mL of QSHs prior to bioprinting, and then the obtained bio-ink mixture was printed immediately.

Bioprinting

The cell-free bio-ink and cell-laden constructs were printed using the Axodual 3D-Bioprinter (Fig. 1a), where SolidWorks and Repetier Host software were used for designing and slicing the constructs. Bioprinting of the QSH bio-ink was performed by using a 25-gauge plastic dispensing tip on microscope slides to allow easy visualization by fluorescence microscopy (Fig. 1b). The constructs were bioprinted at room temperature at 1.6 cm width and length, and the layer height was 0.1 mm. The printing speed for perimeter and infill printing was 10 mm s⁻¹. The infill pattern was a grid structure for square models and the infill density was 40% (Fig. 1c and d). The grid structure was preferred as an infill pattern since porous structures improve the cell viability by allowing oxygen and mass transfer in tissue engineering applications.³⁴ The flow rate of the dispensed bio-ink was controlled by tuning the printing pressure between 1.6 and 7.2 psi.

Both NIH-3T3 mouse fibroblast cells and MDA-MB-231 GFP human breast cancer epithelial cells were used for cell-based bioprinting studies. Cells were cultured and expanded in Dulbecco's modified Eagle's medium (DMEM) supplemented with 10% fetal bovine serum (FBS) and 1% penicillin-streptomycin (P/S). Cells were harvested, when 80–90% confluency was obtained, using 0.25% trypsin-EDTA. Prior to bioprinting, 5 \times 10⁶ cells were added to 1 mL of QSH (100 mg mL⁻¹) and EDC-NHS. The cell-scaffold complexes were bioprinted with a 25-gauge plastic dispensing tip by applying pressure in the range between 6.5 and 7.2 psi. Following the crosslinking of the QSH, the cell-laden constructs were rinsed with PBS to remove unreacted EDC-NHS and visualized by fluorescence microscopy. The cell viability and proliferation analyses were performed using the live/dead viability assay and visualized by fluorescence microscopy for short-term (day 1–7) and long-term (week 1–8). Cells on the QSH scaffolds were compared with the 2D control group, which is maintained on tissue culture polystyrene (TCPS).

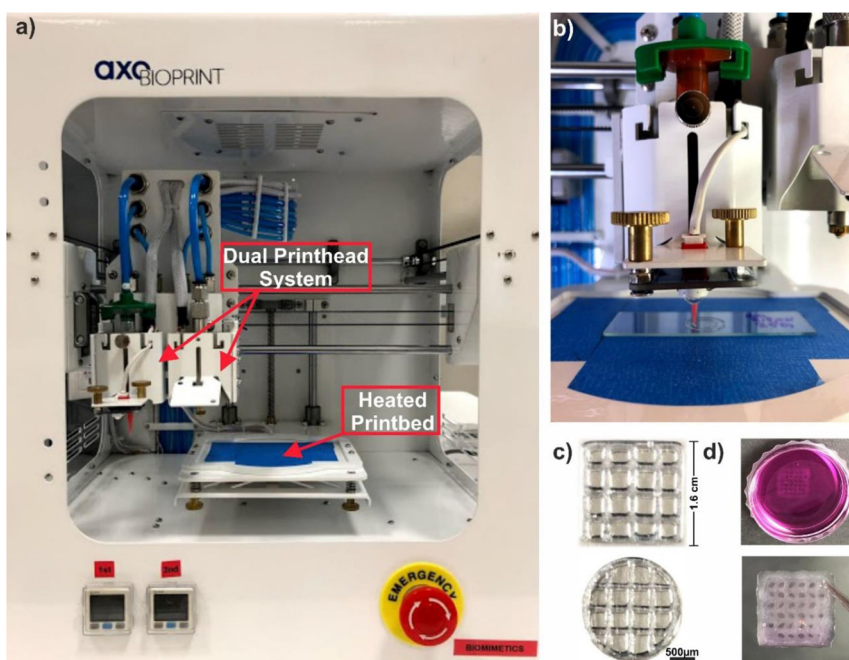


Fig. 1 (a) General view of a 3D-bioprinter, (b) printhead system, (c) 3D bioprinted constructs (scale bar: 500 μm), and (d) conditioned constructs in cell media.

Printability analysis and characterization of the bioprinted constructs

Optimization of the bioprinting parameters for the QSH bio-ink was carried out using a linear filament model for varied pressure values (1.6–7.2 psi) and QSH concentrations (40, 50, 60, and 100 mg mL^{-1}), and the bioprinted constructs were visualized by fluorescence microscopy (Zeiss Axio Observer). The filament thicknesses were measured using Image J Software (NIH). Square models with a grid structure were also bioprinted and visualized for qualitative printability analysis. The uniformity and pore factor were measured for quantitative analysis using Image J, calculated using eqn (1) and (2),^{35,36} and the obtained data were plotted using OriginPro (Northampton, MA) software. The results represent the mean value of three individual data sets for each parameter and formulation.

$$\text{Uniformity Factor (U)} = \frac{\text{Length of the practical line}}{\text{Length of the theoretical smooth line}} \quad (1)$$

$$\text{Pore Factor (Pr)} = \frac{(\text{Peripheral length})^2}{16 \times \text{Pore Area}} \quad (2)$$

Pores, corners, junctions, and cross-sections of the bioprinted constructs were observed by scanning electron microscopy (SEM; FEI Quanta 250 FEG). The pore angle of grids for 1-layer deposition for each concentration and the layer height of cross-sections for 2-, 3- and 4-layer deposition of the QSH bio-ink (100 mg mL^{-1}) were analyzed using ImageJ.

Rheological analysis of the QSH was performed to evaluate the viscosity for each concentration. 40, 50, 60 and 100 mg mL^{-1} QSH samples were examined using a Haake Viscotester VT550 (Thermo Fisher Scientific) within 0–1000 s^{-1} shear rate at a constant temperature (25 $^{\circ}\text{C}$).³⁷

The water uptake capacity of the bioprinted construct was assessed by comparing the wet and dry mass before and after immersion in PBS. Through this experiment, 100 mg mL^{-1} QSHs were bioprinted and crosslinked. These scaffolds were dried out overnight in a desiccator and weighed. Then, they were immersed in PBS for 0–24 h and then weighed. The water uptake capacity was calculated using the formula $((W_t - W_d)/W_d) \times 100$, where W_t represents the wet weight after immersion in PBS and W_d represents the dry weight of scaffolds.^{26,38}

The total adsorbed protein amount on the bioprinted constructs was determined by the bicinchoninic acid (BCA) (Pierce™, Thermo Scientific) assay. To investigate the protein adsorption capacity of the scaffold material, 0–2000 $\mu\text{g mL}^{-1}$ stock protein solutions were prepared by solubilizing bovine serum albumin (BSA).^{39,40} After immersion of QSHs into protein solutions, the adsorbed BSA was solubilized from QSH scaffolds with SDS, and the absorbance values were measured using a UV/Vis Microplate Spectrophotometer (Fisher Scientific™ accuSkan™ GO) at 562 nm. The obtained results were plotted using OriginPro Software.

Statistical analysis

Linear and pore regularity analyses were performed using 3 datasets and expressed as mean value \pm SD. The pore angle

and layer height measurements were also performed using 3 images obtained by SEM observation. Rheological analysis, water uptake capacity determination and protein adsorption assay were performed using 3 datasets, and the results are given as mean value \pm SD.

Results and discussion

Printability analysis

Printability of the QSH bio-ink was assessed by printing linear filament models at a pressure range of 1.6–7.2 psi for 40–100 mg mL⁻¹ QSH concentrations. Dispensing pressure is one of the important bioprinting parameters including feed rate, concentration and extruder diameter.⁴¹ To achieve printability, the dispensing pressure should overcome the surface tension of the bio-ink material. To investigate the printability pressure *versus* hydrocolloid concentration, screening that produces regular, irregular, thick, and unextrudable filaments was performed as shown in Fig. 2. 40 mg mL⁻¹ QSH bio-ink formed regular filaments in the range 1.2–2.0 psi, and above 2.0 psi, the filament became thicker and irregular (Fig. 2a). Also, 50 mg mL⁻¹ QSH formed regular filaments between 3.0 and 4.5 psi, and below this range unextrudable and thicker filament structures were obtained (Fig. 2b). 4.0 and 5.0 psi pressure values are appropriate for bioprinting of regular filament structures when 60 mg mL⁻¹ QSH was used (Fig. 2c). After 5.0 psi, an increase in pressure resulted in a thicker fila-

ment, which is in correlation with the literature. Previous bioprinting studies showed that a pressure increment thickens the lines/filaments.^{42,43} 100 mg mL⁻¹ QSH was uniformly bioprinted between 6.8 and 7.2 psi (Fig. 2d). As expected, the viscosity is increased with increasing concentration, and increased viscosity leads to increased printing pressures (Fig. 2e); however, it favors the biofabrication of regular linear structures and filaments.^{44,45} Higher viscosity is a more preferred parameter for bioprinting applications, since it results in higher printing stability and ultra-controllability on printed filaments.⁴⁵ In addition to qualitative assessment of printability, quantitative analysis was also performed to obtain the optimized pressure value. The width of the bioprinted filaments was visualized by fluorescence imaging and analyzed using Image J (Fig. 2f).

The rheological analysis results of QSH are given in Fig. 2g. As expected, an increase in concentration led to an increase in the viscosity of hydrocolloids. QSH obeys the power-law model. Consistency coefficients for this model were calculated using the viscosity and shear rate; they were 19.34 ± 2.64 , 28.11 ± 3.53 , 34.95 ± 4.92 , and 164 ± 17.17 for 40, 50, 60 and 100 mg mL⁻¹ QSH, respectively, which indicated the apparent increment in viscosity at 100 mg mL⁻¹. The viscosity for 100 mg mL⁻¹ was around 150 Pa s when the shear rate was 1 s⁻¹, and this value is in the appropriate range (3×10^{-2} – 6×10^4 Pa s) for extrusion-based bioprinting.^{11,46}

After optimizing printing parameters, the assessment of QSH printability was further controlled by printing complex

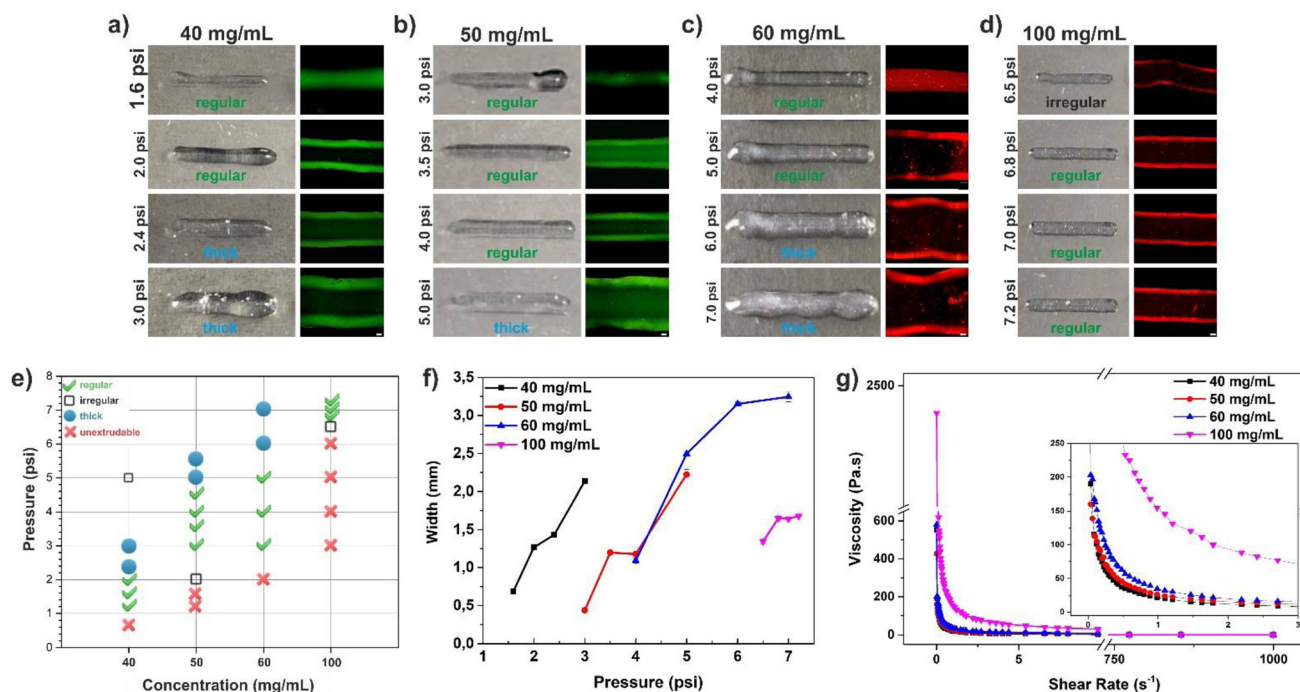


Fig. 2 Printability analysis images as line models of (a) 40, (b) 50, (c) 60, and (d) 100 mg mL⁻¹ using a 25G dispensing tip (scale bar: 200 μ m); (e) summarizing plot for printability analysis of 40, 50, 60, and 100 mg mL⁻¹ QSH at varied pressures. (f) width vs. pressure graph for each concentration at varied pressure values and (g) rheological analysis of 40, 50, 60, and 100 mg mL⁻¹ QSH between 0 and 1000 s⁻¹ shear rate.

3D models with grid infill. For qualitative analysis, junctions, pores, and channels were visualized by fluorescence microscopy. When 40 mg mL⁻¹ QSH and 1.6 psi dispensing pressure were used, square-shaped pores, uniform channels, and sharp junctions were obtained compared to higher-pressure values of the same concentration (Fig. 3a). 50 mg mL⁻¹ QSH provided good square-shaped pores, regular lines, and sharp junctions when 3.0 psi was used; however the regularity of the pores diminished with increasing pressure (Fig. 3b). 60 mg mL⁻¹ QSH revealed regular pores, uniform lines, and sharp junctions when 4.0 psi was used. On the other hand, higher-pressure values disrupted the regular shape of pores and formed thickened lines (Fig. 3c). 6.5 and 6.8 psi were the optimum dispensing pressure values for 100 mg mL⁻¹ QSH. Above these pressure values, square-

shaped pores started to lose their uniformity and regularity, and also lines were thickened (Fig. 3d).

For quantitative analysis of printability, uniformity and pore factors were measured and calculated using eqn (1) and (2). The uniformity did not significantly change between 1.6 psi and 2.4 psi for 40 mg mL⁻¹ QSH; however, there was an important alteration at 3.0 psi (Fig. 3e). 50 mg mL⁻¹ QSH showed linear uniformity when 3.0 psi was used, and above 3.0 psi the linear uniformity diverged from 1.0. 60 mg mL⁻¹ QSH showed appropriate linear uniformity, which is around 1.0 at 5.0 psi and above. For 100 mg mL⁻¹ QSH, similar linear uniformity was obtained which was close to 1.0 for all pressure values varying between 6.5 and 7.2.

Furthermore, the pore regularity was calculated using the peripheral length and pore area. All pore regularity factors

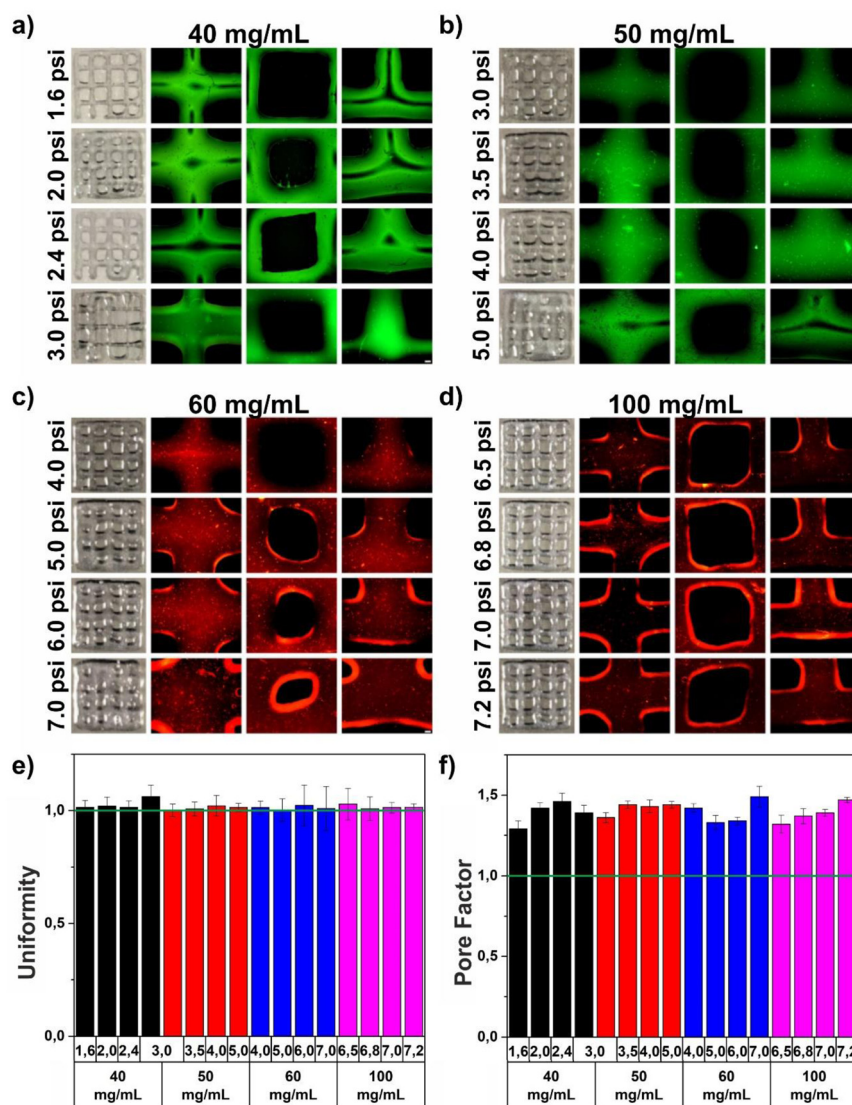


Fig. 3 Biprinted constructs (a) 40 mg mL⁻¹ QSH between 1.6 and 3 psi, (b) 50 mg mL⁻¹ QSH with 3.0, 3.5, 4.0 and 5.0 psi, (c) 60 mg mL⁻¹ QSH between 4.0 and 7.0 psi, and (d) 100 mg mL⁻¹ at 6.5, 6.8, 7.0, and 7.2 psi and fluorescence microscopy images of corners, pores, and junctions (scale bar: 200 μ m), (e) uniformity and (f) pore factor for each concentration calculated using their fluorescence microscopy images.

were bigger than 1.0. However, that closer to 1.0 was the optimum and the most appropriate pressure value for each concentration is 1.6 psi for 40 mg mL⁻¹, 3.0 psi for 50 mg mL⁻¹, 5.0 psi for 60 mg mL⁻¹, and 6.5 psi for 100 mg mL⁻¹ QSH (Fig. 3f). These results quantitatively confirmed the optimal dispensing pressure values, which were optimized qualitatively in the previous step according to Fig. 3a–d. Overall, it was confirmed that all optimized bio-ink formulations and optimized dispensing pressure values were suitable for the biofabrication of regular and uniform 3D structures. Further studies were conducted using optimum parameters as 6.5–7.2 psi for 100 mg mL⁻¹ QSH.

Characterization of the bioprinted constructs

In this study, the EDC–NHS coupling methodology was implemented for crosslinking the bioprinted QSHs. Addition of EDC–NHS solution to QSH lowered the viscosity of the gel and for this reason, the required bioprinting pressure decreased for each concentration. The bioprinting of the QSH with EDC–NHS crosslinking was completed in 15 minutes and the scaffolds were incubated in ultra-pure water. Fully crosslinked constructs were analyzed by SEM, where pores and junctions were imaged (Fig. 4a). The pore angle was then analyzed using ImageJ for each sample. The regular pore

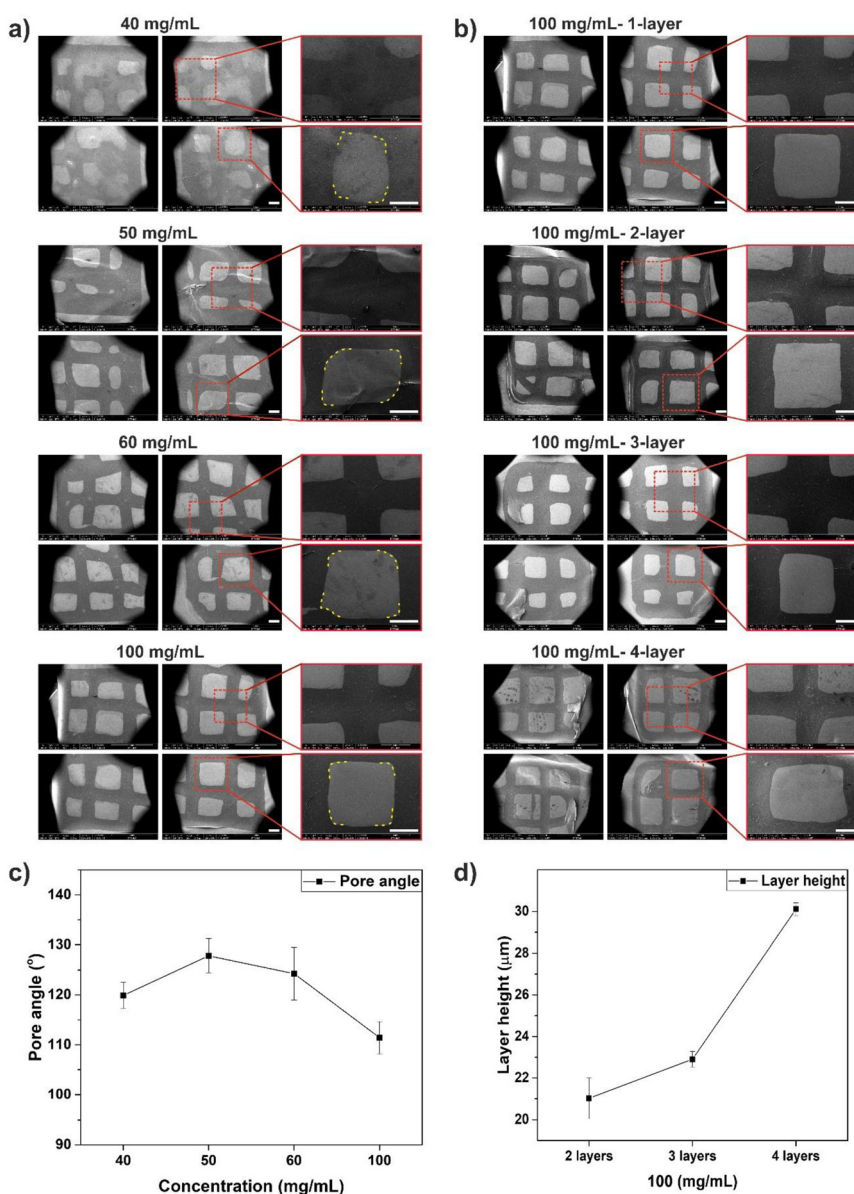


Fig. 4 SEM analysis results for (a) 40, 50, 60, and 100 mg mL⁻¹, (b) 100 mg mL⁻¹ (1-, 2-, 3-, and 4-layer) (scale bar: 1 mm), (c) pore angles, and (d) layer heights of 2-, 3-, and 4-layer 100 mg mL⁻¹ QSH.

angle should be 90° according to the scaffold design. The uniformity of pores increased with the increase in concentration. With increasing viscosity, the pore angle of the scaffold was close to 90° (Fig. 4c). An increase in concentration, and hence in viscosity, resulted in regular shape and pores in which collapse and deformation were not observed.⁴¹

For further assessment of printability, multi-layer forms of 100 mg mL^{-1} QSHs were bioprinted and analyzed by SEM (Fig. 4b). The layer heights were measured from cross-sectional images (Fig. 4d), and they were around $21 \mu\text{m}$, $22.5 \mu\text{m}$, and $30 \mu\text{m}$ respectively for 2-, 3-, and 4-layer forms of 100 mg mL^{-1} QSH.

In tissue engineering, water uptake capacity is an important parameter for scaffold design, and it can be controlled by varying the crosslinking density and percent porosity.⁴⁷ The water uptake capacity of 100 mg mL^{-1} QSH scaffold was measured by weighing the scaffold before and after 0–24 h immersion in PBS. As expected, the water uptake capacity of QSH linearly increased with the incubation time until 1 h (Fig. 5a), and then swelling equilibrium was reached between 5 and 7 h. After 7 h, partial deswelling around 7.5% was observed. At the equilibrium point, QSH held 20.2 times more water than its own mass when immersed in PBS for 7 h, while 18.3 fold was reached after 24 h immersion in PBS, which is a remarkable water uptake capacity for hydrogels.^{48,49}

Since protein adsorption is generally ensured by cell adhesion,⁵⁰ protein adsorption analysis was performed using the BCA assay to test the cell adhesion capability for 3D cell culture. Briefly, 100 mg mL^{-1} QSHs were bioprinted and cross-linked by EDC-NHS, and then they were immersed in BSA solutions ($25\text{--}2000 \mu\text{g mL}^{-1}$); after incubation, the adsorbed proteins were solubilized by SDS. The amount of adsorbed protein on the bioprinted QSH increased with the increase of

protein concentration and reached a maximum at $225 \mu\text{g mL}^{-1}$ (Fig. 5b).

3D Cell Culture and Viability Analysis

Bioprinting of cells into hydrogels is a trending technique since the biocompatibility and convenience of hydrogels provide sophisticated models and constructs. 3D cell bioprinting application gives similar microenvironments physiologically.⁵¹ For this reason, the bioprinting ability of cells into hydrogels is important. Cell viability during this bioprinting process is the key point and can be kept under control by tuning the bioprinting pressure and diameter of the nozzle.⁵² For 3D bioprinting MDA-MB-231 GFP containing QSH (100 mg mL^{-1}) bio-ink was prepared prior to bioprinting. Bioprinting of the bio-ink was performed at various pressure values, and then channels, junctions and pores were analyzed by fluorescence microscopy (Fig. 6a and b). According to the literature, the cell viability was significantly reduced when the bioprinting pressure was high.⁵² Also, an increase in pressure disrupts pore, channel, and junction uniformity and causes an increase in the number of dead cells. Therefore, the bioprintability of concentrated QSH at a low pressure, such as 6.5 psi, provided an advantage as a bio-ink.

For cell viability and biocompatibility assessment of the QSH, NIH-3T3 cells were cultured on QSH scaffolds for a short (Fig. 7) and long time (Fig. 8). Cell viability and proliferation assays on the QSH scaffolds were carried out and controlled by the live-dead assay. During 3D culturing (Fig. 7 and 8), the QSH promoted cells to form spheroids which is also supported by previous reports.²⁶ Compared to the QSH, cells proliferated over each other in the 2D control group. On day 1 smaller 3D cellular structures were observed, and later on day 5 and day 7 they started to associate and fuse to form larger 3D cellular structures (Fig. 7a–c). Relative cell viability was calculated

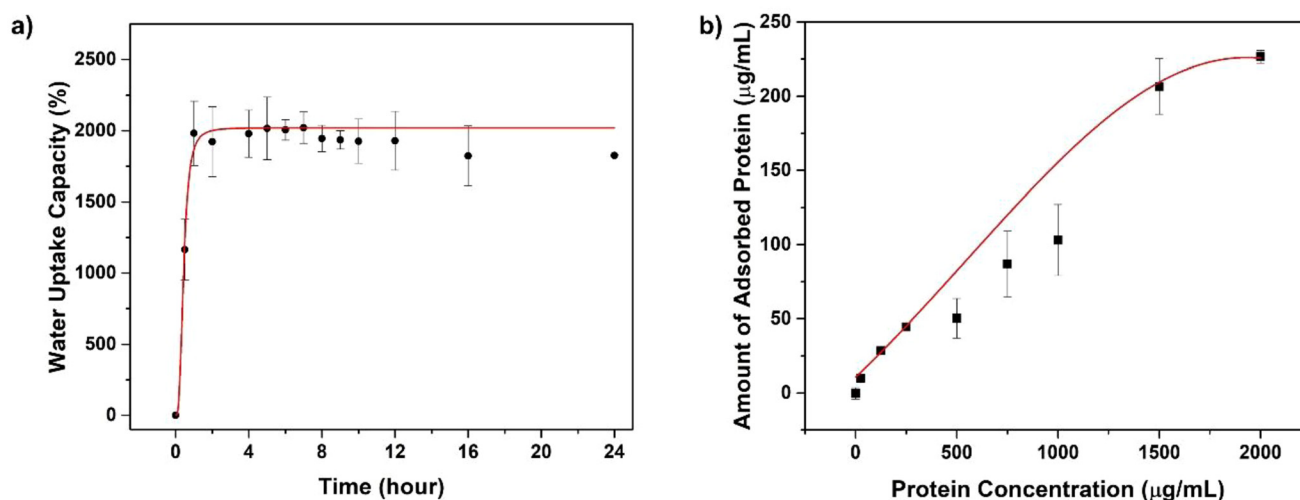


Fig. 5 (a) Water uptake capacity and (b) protein adsorption results of 100 mg mL^{-1} QSH.

using short-term live-dead images. Fig. 7d shows superior cell proliferation and viability which is higher than 95% for the QSH. High cell viability and proliferation were observed even

for 8 weeks culture time (Fig. 8), indicating the biocompatibility and suitability of the QSH as a promising bio-ink in the field of tissue engineering.

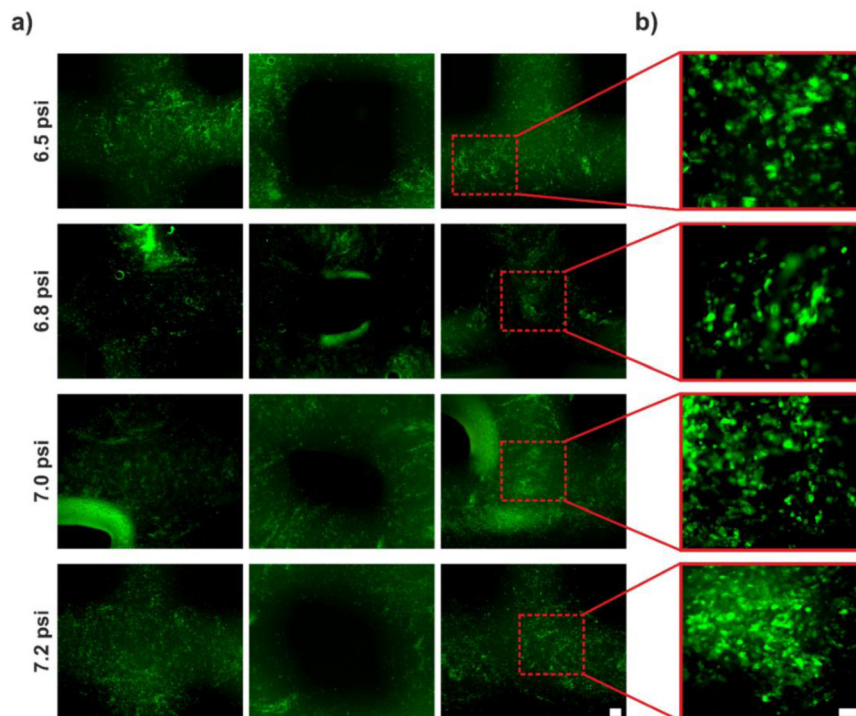


Fig. 6 Fluorescence microscopy images of GFP MDA-MB-231 cell bioprinting with 100 mg mL⁻¹ QSH using a 25G dispensing tip. (a) The general junction, pore, and corner view with cells (scale bar: 200 μm) and (b) the images of GFP cells in bioprinted QSHs at a higher magnification (scale bar: 100 μm).

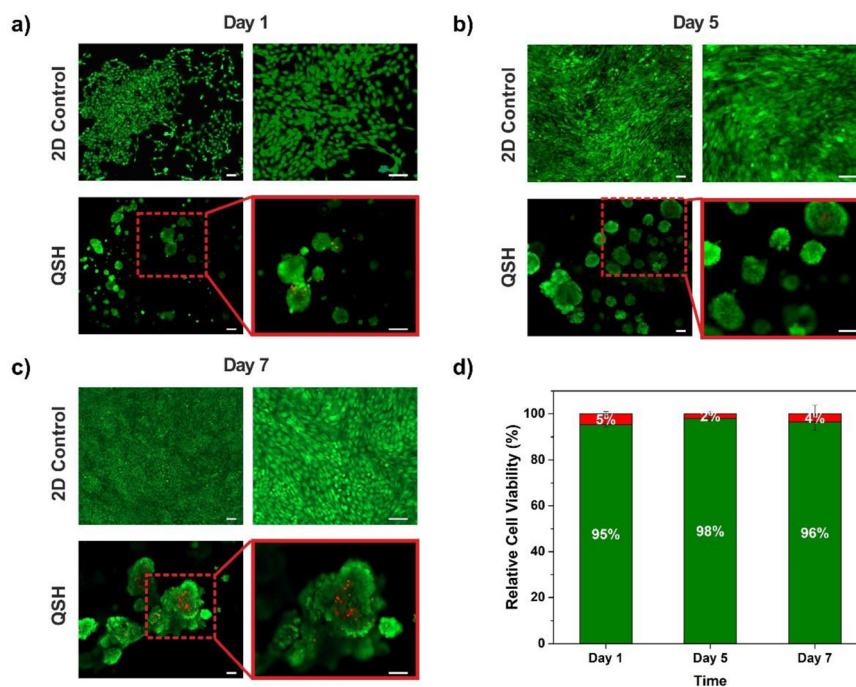


Fig. 7 Short-term cell viability images of NIH-3T3 cells on bioprinted QSH scaffolds (a) day 1, (b) day 5, and (c) day 7 (scale bar: 100 μm); (d) relative cell viability results (green: live cells, red: dead cells).

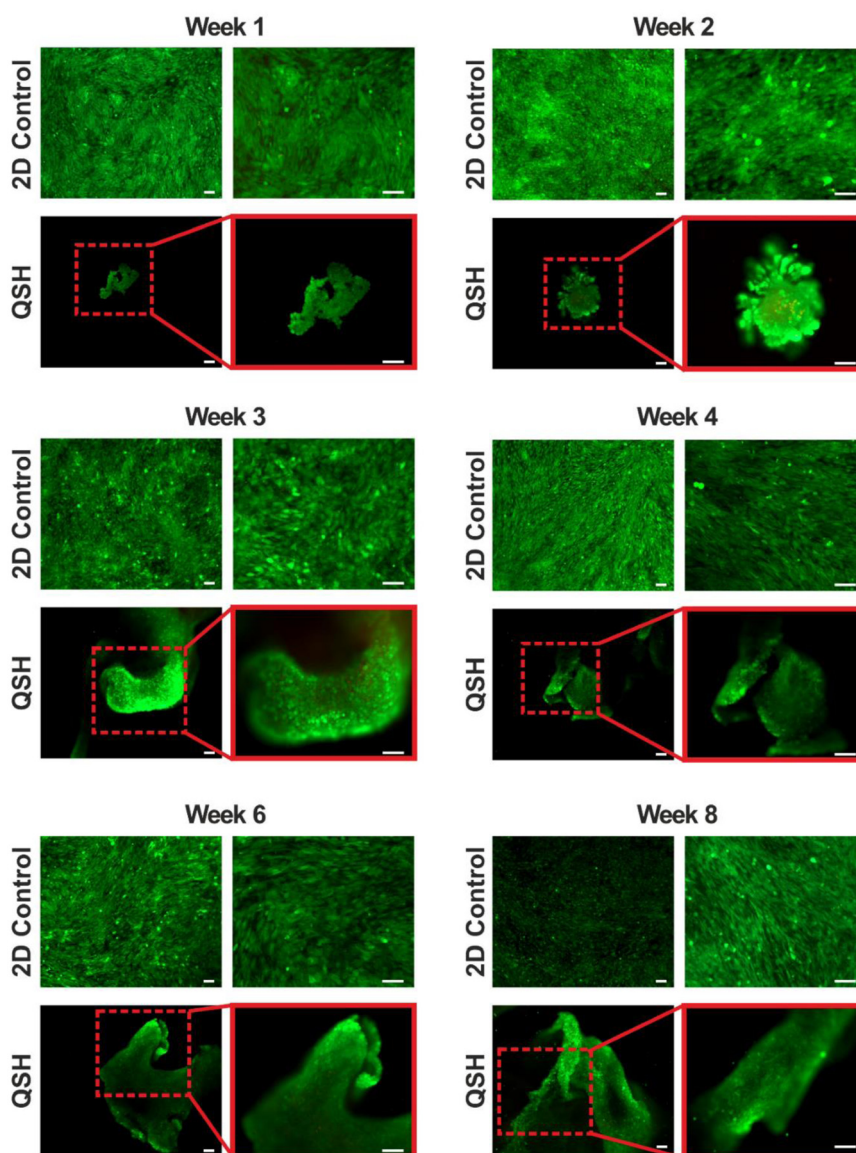


Fig. 8 Long-term cell viability images of NIH-3T3 cells on bioprinted QSH scaffolds (scale bar: 100 μm).

Conclusions

In the present study, a hydrocolloid obtained from quince seeds was studied as a bio-ink in 3D bioprinting applications. To achieve this goal, printability analysis through linear, pore regularity, and SEM analysis, water uptake capacity determination, and protein adsorption capacity analyses were performed. In addition, the biocompatibility of the QSH bio-ink was evaluated by cell proliferation and viability analysis. At the end, the appropriate concentration of the QSH and the optimal printing pressure were determined to be 100 mg mL⁻¹ and 6.5 psi, respectively. The required printing pressure was consistent with the suitable cell bioprinting pressure in the literature.⁵³ The water uptake capacity of the QSH was 20.2-fold its own weight and was higher rather than other hydrogels that are used for soft tissue engineering.^{48,49,54} In addition, the fast and easy

gelling feature of the QSH and the ability to be crosslinked with a non-toxic methodology are the promising features of the QSH as a bio-ink. Furthermore, short and long-term cell culture studies demonstrated that the QSH has excellent biocompatibility and its high viability has been observed for 8 weeks. The development and characterization of a new-generation bio-ink from the QSH were studied for the first time, and this novel bio-ink is a promising scaffold material in scaffold-based tissue engineering and 3D bioprinting applications.

Author contributions

Özüm Yildirim: investigation, formal analysis, and writing – original draft. Ahu Arslan-Yildiz: conceptualization, supervision, and writing – review & editing.

Conflicts of interest

There are no conflicts to declare.

Acknowledgements

This study was financially supported by TUBITAK (120C155). The authors gratefully acknowledge the TUBITAK 2247-A National Leading Researchers Program.

The authors acknowledge İzmir Institute of Technology Biotechnology and Bioengineering Research and Application Center and İzmir Institute of Technology Materials Research Center for the instrumental facilities provided to accomplish this study. We thank Prof. Dr Sevcan Ünlütürk and Berkay Berk for rheological analysis and their feedback.

References

- B. K. Gu, D. J. Choi, S. J. Park, M. S. Kim, C. M. Kang and C. H. Kim, *Biomater. Res.*, 2016, **20**, 12.
- P. S. Gungor-Ozkerim, I. Inci, Y. S. Zhang, A. Khademhosseini and M. R. Dokmeci, *Biomater. Sci.*, 2018, **6**, 915–946.
- Y. Fang, Y. Guo, T. Liu, R. Xu, S. Mao, X. Mo, T. Zhang, L. Ouyang, Z. Xiong and W. Sun, *Chin. J. Mech. Eng. Addit. Manuf. Front.*, 2022, **1**, 100011.
- C. C. Piras, S. Fernández-Prieto and W. M. De Borggraeve, *Biomater. Sci.*, 2017, **5**, 1988–1992.
- S. Panda, S. Hajra, K. Mistewicz, B. Nowacki, P. In-na, A. Krushynska, Y. Kumar Mishra and H. Joon Kim, *Biomater. Sci.*, DOI: [10.1039/D2BM00797E](https://doi.org/10.1039/D2BM00797E).
- A. Arslan-Yildiz, R. El Assal, P. Chen, S. Guven, F. Inci and U. Demirci, *Biofabrication*, 2016, **8**, 014103.
- S. Heid and A. R. Boccaccini, *Acta Biomater.*, 2020, **113**, 1–22.
- A. N. Leberfinger, S. Dinda, Y. Wu, S. V. Koduru, V. Ozbolat, D. J. Ravnic and I. T. Ozbolat, *Acta Biomater.*, 2019, **95**, 32–49.
- W. Sun, B. Starly, A. C. Daly, J. A. Burdick, J. Groll, G. Skeldon, W. Shu, Y. Sakai, M. Shinohara, M. Nishikawa, J. Jang, D. W. Cho, M. Nie, S. Takeuchi, S. Ostrovidov, A. Khademhosseini, R. D. Kamm, V. Mironov, L. Moroni and I. T. Ozbolat, *Biofabrication*, 2020, **12**(2), 022002.
- W. L. Ng, J. M. Lee, W. Y. Yeong and M. Win Naing, *Biomater. Sci.*, 2017, **5**, 632–647.
- M. Hospodiuk, M. Dey, D. Sosnoski and I. T. Ozbolat, *Biotechnol. Adv.*, 2017, **35**, 217–239.
- D. Chimene, K. K. Lennox, R. R. Kaunas and A. K. Gaharwar, *Ann. Biomed. Eng.*, 2016, **44**, 2090–2102.
- L. Moroni, J. A. Burdick, C. Highley, S. J. Lee, Y. Morimoto, S. Takeuchi and J. J. Yoo, *Nat. Rev. Mater.*, 2018, **3**, 21–37.
- V. H. M. Mouser, R. Levato, A. Mensinga, W. J. A. Dhert, D. Gawlitza and J. Malda, *Connect. Tissue Res.*, 2020, **61**, 137–151.
- M. Askari, M. Afzali Naniz, M. Kouhi, A. Saberi, A. Zolfagharian and M. Bodaghi, *Biomater. Sci.*, 2021, **9**, 535–573.
- L. Stoloff, *Adv. Carbohydr. Chem.*, 1958, **13**, 265–287.
- S. Van Vlierberghe, P. Dubruel and E. Schacht, *Biomacromolecules*, 2011, **12**, 1387–1408.
- J. H. Park, G. Saravanakumar, K. Kim and I. C. Kwon, *Adv. Drug Delivery Rev.*, 2010, **62**, 28–41.
- T. R. Hoare and D. S. Kohane, *Polymer*, 2008, **49**, 1993–2007.
- K. Ganguly, K. Chaturvedi, U. A. More, M. N. Nadagouda and T. M. Aminabhavi, *J. Controlled Release*, 2014, **193**, 162–173.
- Z. Wei, J. H. Yang, Z. Q. Liu, F. Xu, J. X. Zhou, M. Zrínyi, Y. Osada and Y. M. Chen, *Adv. Funct. Mater.*, 2015, **25**, 1352–1359.
- L. Long, W. Liu, C. Hu, Li Yang and Y. Wang, *Biomater. Sci.*, 2022, **10**, 4058–4076.
- S. S. Stalling, S. O. Akintoye and S. B. Nicoll, *Acta Biomater.*, 2009, **5**, 1911–1918.
- S. B. Deshmukh, A. M. Kulandainathan and K. Murugavel, *Biomater. Sci.*, DOI: [10.1039/D2BM00820C](https://doi.org/10.1039/D2BM00820C).
- V. D. Prajapati, G. K. Jani, N. G. Moradiya and N. P. Randeria, *Carbohydr. Polym.*, 2013, **92**, 1685–1699.
- M. Guzelgulgen, D. Ozkendir-Inanc, U. H. Yildiz and A. Arslan-Yildiz, *Int. J. Biol. Macromol.*, 2021, **180**, 729–738.
- M. U. Ashraf, M. A. Hussain, G. Muhammad, M. T. Haseeb, S. Bashir, S. Z. Hussain and I. Hussain, *Int. J. Biol. Macromol.*, 2017, **95**, 138–144.
- M. U. Ashraf, M. A. Hussain, S. Bashir, M. T. Haseeb and Z. Hussain, *J. Drug Delivery Sci. Technol.*, 2018, **45**, 455–465.
- M. R. Vignon and C. Gey, *Carbohydr. Res.*, 1998, **307**, 107–111.
- A. Moghbel and M. Tayebi, *Jundishapur J. Nat. Pharm. Prod.*, 2015, **10**(3), DOI: [10.17795/jjnpp-2539](https://doi.org/10.17795/jjnpp-2539).
- L. Wang, H. M. Liu, C. Y. Zhu, A. J. Xie, B. J. Ma and P. Z. Zhang, *Carbohydr. Polym.*, 2019, **209**, 230–238.
- R. Onbas and A. A. Yildiz, *ACS Appl. Bio Mater.*, 2021, **4**, 1794–1802.
- M. A. Hussain, G. Muhammad, M. T. Haseeb and M. N. Tahir, *Functional biopolymers*, 2019, 127–148.
- S. J. Hollister, *Nat. Mater.*, 2005, **4**, 518–524.
- N. Soltan, L. Ning, F. Mohabatpour, P. Papagerakis and X. Chen, *ACS Biomater. Sci. Eng.*, 2019, **5**, 2976–2987.
- L. Ouyang, R. Yao, Y. Zhao and W. Sun, *Biofabrication*, 2016, **8**, 035020.
- L. Wang, H. M. Liu, C. Y. Zhu, A. J. Xie, B. J. Ma and P. Z. Zhang, *Carbohydr. Polym.*, 2019, **209**, 230–238.
- A. J. Xie, H. S. Yin, H. M. Liu, C. Y. Zhu and Y. J. Yang, *Carbohydr. Polym.*, 2018, **185**, 96–104.
- L. Jie, *J. Ethnopharmacol.*, 1995, **49**, 57–68.
- K. Cai, J. Bossert and K. D. Jandt, *Colloids Surf., B*, 2006, **49**, 136–144.
- Y. He, F. Yang, H. Zhao, Q. Gao, B. Xia and J. Fu, *Sci. Rep.*, 2016, **6**, 29977.
- B. Webb and B. J. Doyle, *Bioprinting*, 2017, **8**, 8–12.

- 43 W. L. Ng, W. Y. Yeong and M. W. Naing, *Int. J. Bioprint.*, 2016, **2**, 53–62.
- 44 W. Schuurman, P. A. Levett, M. W. Pot, P. R. van Weeren, W. J. A. Dhert, D. W. Hutmacher, F. P. W. Melchels, T. J. Klein and J. Malda, *Macromol. Biosci.*, 2013, **13**, 551–561.
- 45 A. Ribeiro, M. M. Blokzijl, R. Levato, C. W. Visser, M. Castilho, W. E. Hennink and J. Malda, *Biofabrication*, 2017, **10**(1), 014102.
- 46 C. Mandrycky, Z. Wang, K. Kim and D. H. Kim, *Biotechnol. Adv.*, 2016, **34**, 422–434.
- 47 P. Kakkar, S. Verma, I. Manjubala and B. Madhan, *Mater. Sci. Eng., C*, 2014, **45**, 343–347.
- 48 Q. Q. Wang, Y. Liu, C. J. Zhang, C. Zhang and P. Zhu, *Mater. Sci. Eng., C*, 2019, **99**, 1469–1476.
- 49 M. Muhammad, A. Arif, M. Busra Fauzi, A. Nordin, Y. Hiraoka, Y. Tabata, M. Heikal and M. Yunus, *Polymer*, 2020, **12**, 2678.
- 50 P. Roach, D. Eglin, K. Rohde and C. C. Perry, *J. Mater. Sci. Mater. Med.*, 2007, **18**, 1263–1277.
- 51 C. Khatiwala, R. Law, B. Shepherd, S. Dorfman and M. Csete, *Gene Ther. Regul.*, 2012, **7**, 1230004.
- 52 K. Nair, M. Gandhi, S. Khalil, K. C. Yan, M. Marcolongo, K. Barbee and W. Sun, *Biotechnol. J.*, 2009, **4**, 1168–1177.
- 53 K. Buyukhatipoglu, W. Jo, W. Sun and A. M. Clyne, *Biofabrication*, 2009, **1**(3), 035003.
- 54 O. Okay, *Hydrogel sensors and actuators*, Springer, 2009, pp. 1–14.